SUPPLEMENTAL FIGURES 1-8 AND METHODS

Vitamin B_{12}-dependent taurine synthesis regulates growth and bone mass

Pablo Roman-Garcia[1☯], Isabel Quiros-Gonzalez[1☯], Lynda Mottram[2,3☯], Liesbet Lieben[1,2], Kunal Sharan[1,2], Arporn Wangwiwatsin[1], Jose Tubio[4], Kirsty Lewis[1,2], Debbie Wilkinson[5], Balaji Santhanam[1,6], Nazan Sarper[7], Simon Clare[3], George S. Vassiliou[4], Vidya R. Velagapudi[8], Gordon Dougan[3], Vijay K. Yadav[1,2*]

[1]Systems Biology of Bone Laboratory, [2]Sanger Mouse Genetics Project, Department of Mouse and Zebrafish Genetics,

[3]Pathogen Genetics, and

[4]Human Genetics,

The Wellcome Trust Sanger Institute, Cambridge CB10 1SA, United Kingdom

[5]Instrument Core Facility, University of Aberdeen, Foresterhill, Aberdeen AB25 2ZD, United Kingdom

[6]The Laboratory of Molecular Biology, Medical Research Council, United Kingdom

[7]Pediatrics and pediatric hematology, Kocaeli University Hospital, Kocaeli-41380, Turkey

[8]Metabolomics Unit, Institute for Molecular Medicine Finland FIMM, Helsinki-00014, Finland

☯These authors contributed equally

[*]Corresponding Author:

Vijay K. Yadav Ph.D.

The Morgan Building (N235), The Wellcome Trust Sanger Institute, Cambridge CB10 1SA, United Kingdom. Phone: +44-01223-496948; Fax: +44-01223-496826

email: vy1@sanger.ac.uk

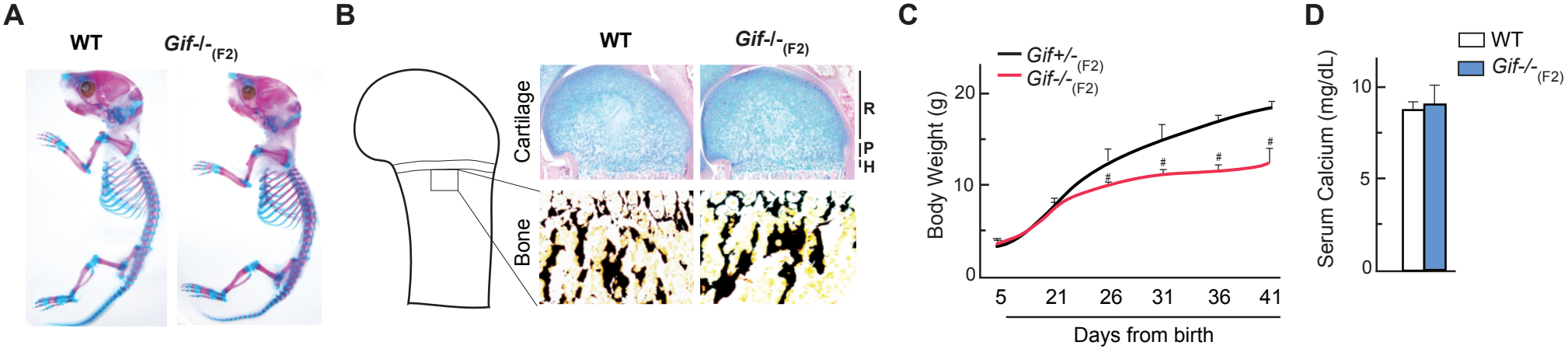

Supplementary figure 1. Vitamin B_{12} deficiency causes growth retardation and low bone mass

(A) Alcian blue/Alizarin red skeletal preparations of newborn WT and *Gif*-/-$_{(F2)}$ mice. (B) Histological analysis of long bone from newborn WT and Gif-/-(B12Deficient) mice. Growth plate architecture (Top panel, magnification 5X): R, Resting chondrocytes; P, Proliferating chondrocytes; H, Hypertrophic chondrocytes. VonKossa analysis of the primary spongiosa (Bottom panel) Magnification: 40X. (C) Growth curve analysis of *Gif*+/-$_{(F2)}$ and *Gif*-/-$_{(F2)}$ mice derived from *Gif*-/-$_{(F1)}$ mother and *Gif*+/-$_{(F1)}$ father. (D) Serum Calcium levels in WT and *Gif*-/-$_{(F2)}$ mice. All panels # $P < 0.05$; * $P < 0.01$

Figure S1

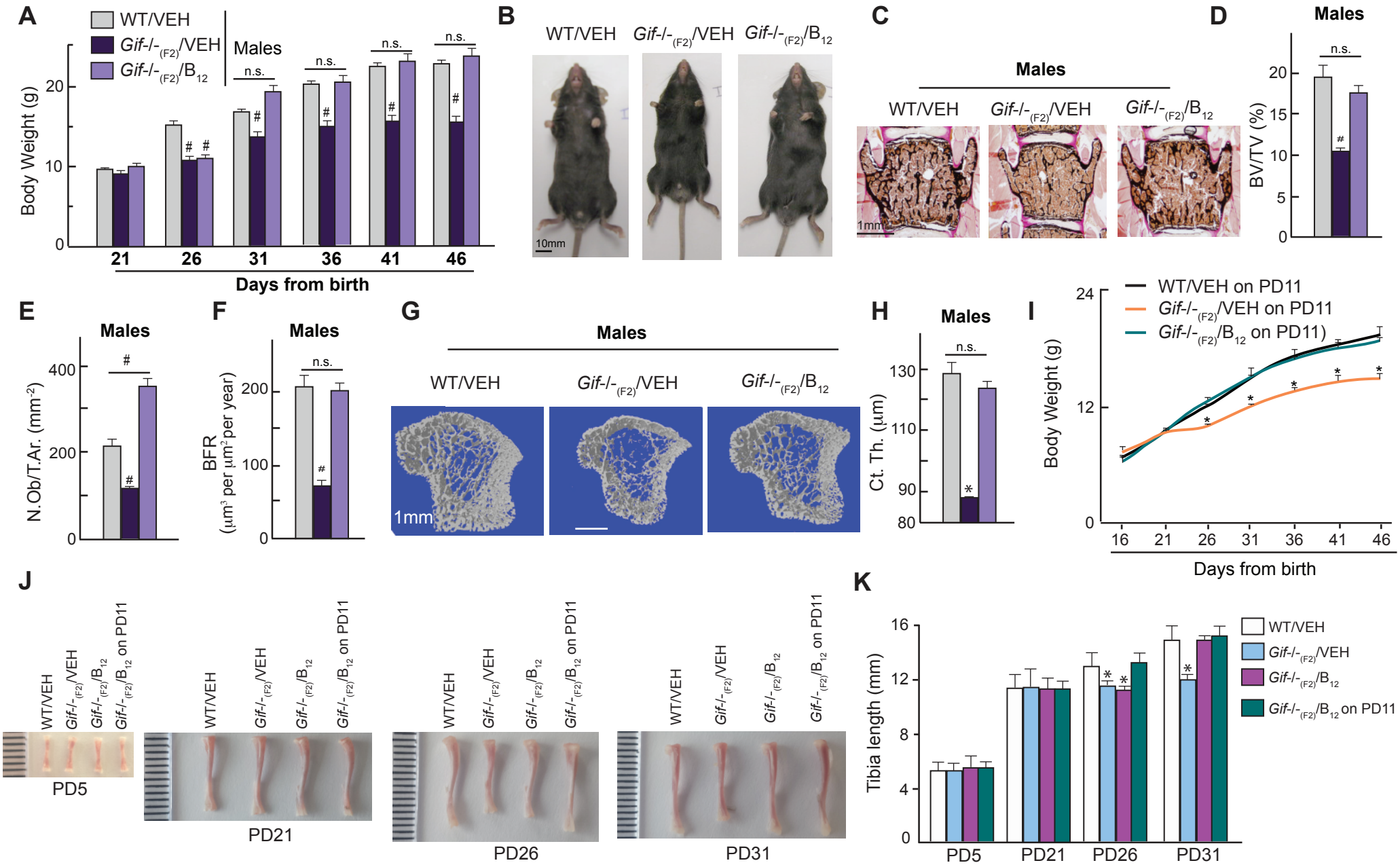

Supplementary figure 2. Maternal B_{12} regulates offspring growth and bone mass and B_{12} deficiency during ageing regulates bone mass independently of body growth. (A) Growth curve analysis of WT, *Gif-/-*$_{(F2)}$/VEH and *Gif-/-*$_{(F2)}$/B_{12} male mice. (B) Photomicrographs of 8-week old WT, *Gif-/-*$_{(F2)}$/VEH and *Gif-/-*$_{(F2)}$/B_{12} male mice. (C-G) Histological analysis of vertebrae of WT, *Gif-/-*$_{(F2)}$/VEH and *Gif-/-*$_{(F2)}$/B_{12} male mice. Mineralized bone matrix is stained in black by von Kossa reagent, BV/TV% (C-D), Ob.N/T.Ar. (E), BFR (F). (G-H) µCT analysis of tibia collected from 8-week old WT, *Gif-/-*$_{(F2)}$/VEH and *Gif-/-*$_{(F2)}$/B_{12} male mice. Representative µCT images from proximal tibia (G) and Cortical thickness analysis (H) is shown. (I) Growth curve analysis of *Gif-/-*$_{(F2)}$ offspring that were injected (s.c.) with VEH or 200 µg of B_{12} on postnatal day 11 (PD11). (J-K) Tibia length analysis on postnatal day (PD) 5, 21, 26 and 31 days in WT, *Gif-/-*$_{(F2)}$/VEH, *Gif-/-*$_{(F2)}$/B_{12} and *Gif-/-*$_{(F2)}$/B_{12} on PD11. Mean values ± SEM are shown. For panels A-H WT/VEH (n=6), *Gif-/-*$_{(F2)}$/VEH (n=5) and *Gif-/-*$_{(F2)}$/B_{12} (n=5). All panels # $P < 0.05$; * $P < 0.01$

Figure S2

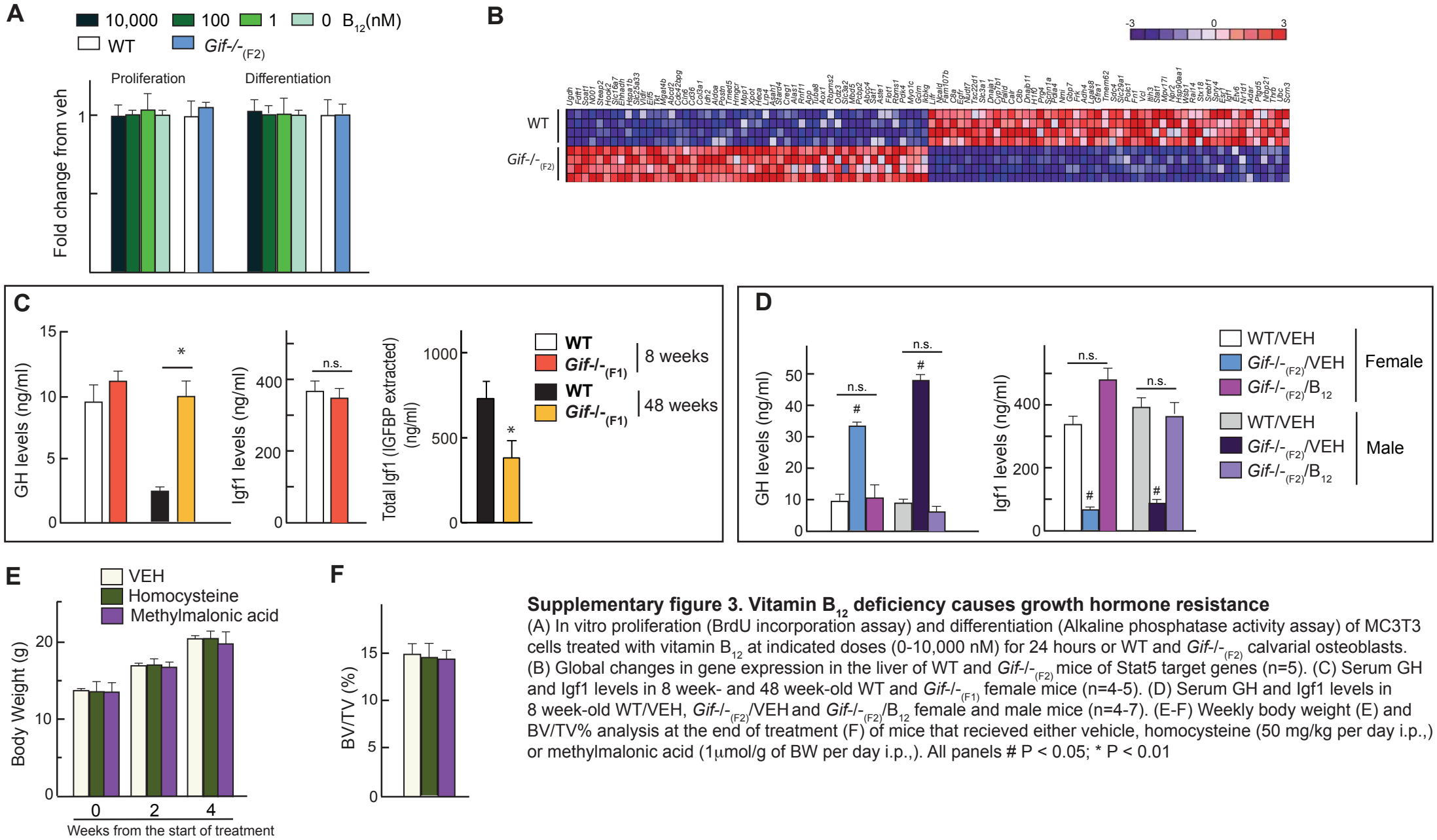

Supplementary figure 3. Vitamin B_{12} deficiency causes growth hormone resistance

(A) In vitro proliferation (BrdU incorporation assay) and differentiation (Alkaline phosphatase activity assay) of MC3T3 cells treated with vitamin B_{12} at indicated doses (0-10,000 nM) for 24 hours or WT and *Gif-/-*$_{(F2)}$ calvarial osteoblasts. (B) Global changes in gene expression in the liver of WT and *Gif-/-*$_{(F2)}$ mice of Stat5 target genes (n=5). (C) Serum GH and Igf1 levels in 8 week- and 48 week-old WT and *Gif-/-*$_{(F1)}$ female mice (n=4-5). (D) Serum GH and Igf1 levels in 8 week-old WT/VEH, *Gif-/-*$_{(F2)}$/VEH and *Gif-/-*$_{(F2)}$/B_{12} female and male mice (n=4-7). (E-F) Weekly body weight (E) and BV/TV% analysis at the end of treatment (F) of mice that recieved either vehicle, homocysteine (50 mg/kg per day i.p.,) or methylmalonic acid (1μmol/g of BW per day i.p.,). All panels # $P < 0.05$; * $P < 0.01$

Figure S3

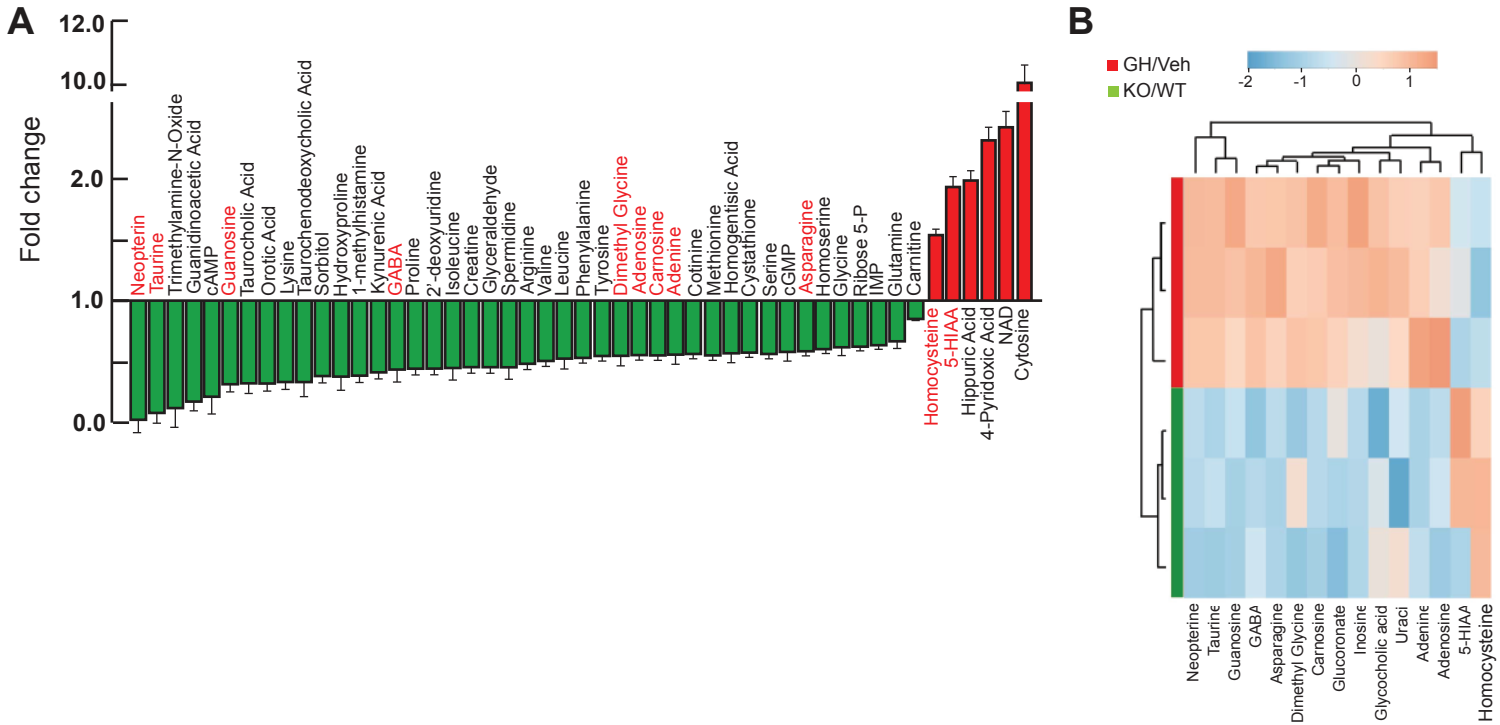

Supplementary figure 4. Metabolomics analysis identifies taurine as a critical metabolite that connects B_{12} deficiency with GH signaling
(A) Fold changes in the metabolites that were ≥50% up or down regulated in the liver of *Gif*-/-$_{(F2)}$ mice compared to the WT mice. Metabolites regulated by GH are highlighted in red font on the list. (B) Supervised hierarchical clustering plot of up or downregulated metabolites from liver samples or from cells treated with GH showing opposite regulation of the same metabolites by B_{12} deficiency or by GH treatment.

Figure S4

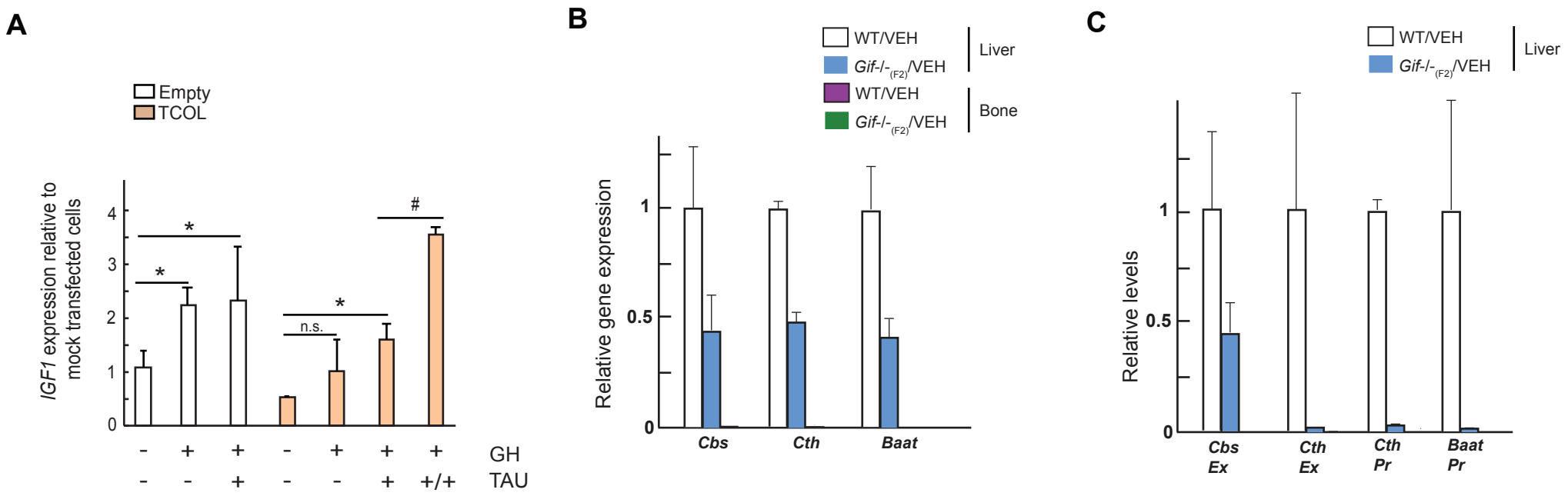

Supplementary figure 5. Growth hormone regulates taurine synthesis in a STAT5 and B_{12} dependent manner
IGF1 gene expression analysis after Taurine (-/+ GH) treatment of control or Tcn2-Oleosin (TCOL) transfected HepG2 cells. Please note that taurine excess can overcome GH resistance observed in the TCOL transfected HepG2 cells. For taurine treatment + indicates 20 mM and ++ indicates 1M. (B) Changes in expression levels of critical enzymes involved in taurine synthesis or metabolism in liver and bone of WT and *Gif*-/-$_{(F2)}$ mice relative to WT liver. (C) ChIP analysis of me2-K36 in promoter (Pr) and Exon 1 (Ex) of critical enzymes involved in taurine synthesis or metabolism in liver of WT and *Gif*-/-$_{(F2)}$ mice. Please note that if a region did not show detectable level of methylation it is not shown. $P < 0.05$; ♯ $P < 0.01$. Error bars: SEM.

Figure S5

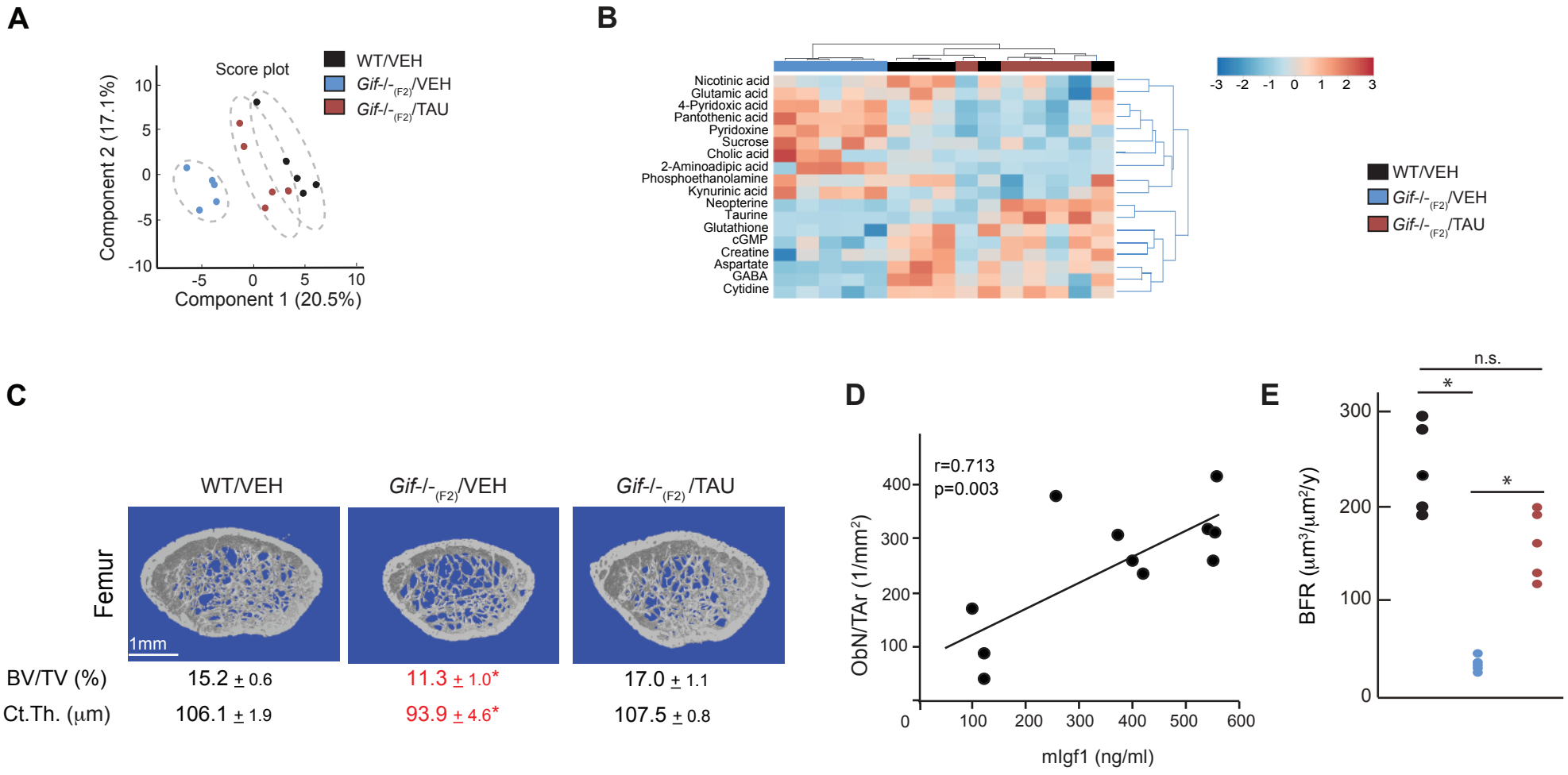

Supplementary figure 6. Taurine prevents growth retardation and osteoporosis in *Gif-/-*$_{(F2)}$ mice

A) Principle component analysis plot from the metabolomics experiment of WT/VEH, *Gif-/-*$_{(F2)}$/VEH and *Gif-/-*$_{(F2)}$/TAU mice showing that WT and *Gif-/-*$_{(F2)}$/TAU mice cluster together. (B) Heatmap representation of significantly altered metabolites by ANOVA analysis of liver metabolomics data from WT, *Gif-/-*$_{(F2)}$/VEH and *Gif-/-*$_{(F2)}$/TAU mice. (C) μCT analysis in the distal femur from WT, *Gif-/-*$_{(F2)}$/VEH and *Gif-/-*$_{(F2)}$/TAU mice showing complete prevention of osteoporosis in long bones following taurine treatment. (D) Pearson correlation scatter plot between ObN/TAr and serum Igf1 levels in taurine-treated mice. (E) Bone formation rate in WT/VEH, *Gif-/-*$_{(F2)}$/VEH and *Gif-/-*$_{(F2)}$/TAU mice. All panels # $P < 0.05$; * $P < 0.01$. Error bars, SEM. n.s., not significant.

Figure S6

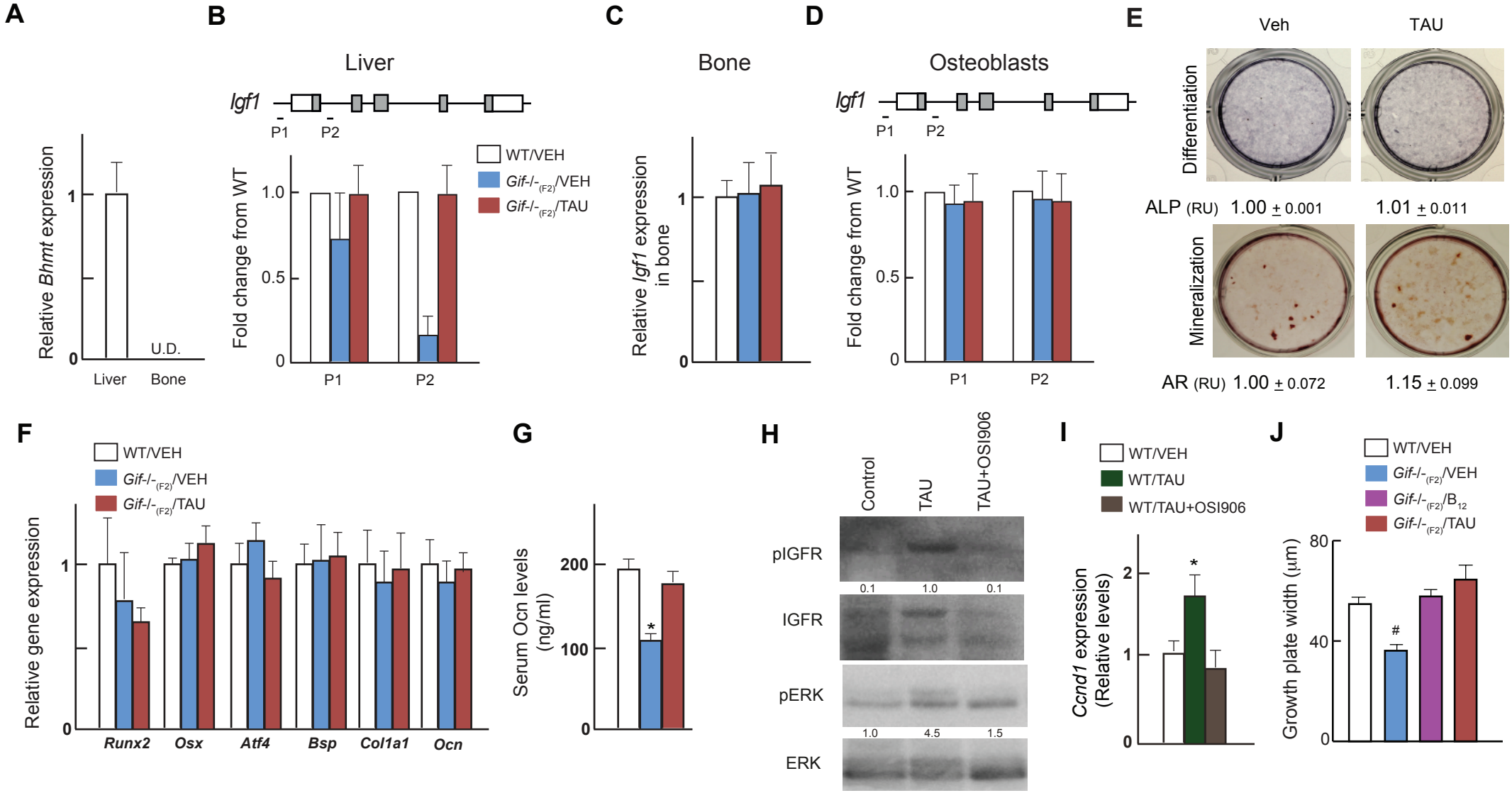

Supplementary figure 7. Taurine increases osteoblast proliferation by increasing Igf1 synthesis and action

(A) Relative *Bhmt* expression in liver and bone. (B) ChIP analysis of me2-K36 in P1 and P2 regions of Igf1 gene in the liver of WT, *Gif-/-*$_{(F2)}$/VEH and *Gif-/-*$_{(F2)}$/TAU mice (WT values set at 1 for each region). (C-D) Relative *Igf1* expression in bone (C) and ChIP analysis of me2-K36 in P1 and P2 regions of *Igf1* gene in osteoblasts (D) of WT, *Gif-/-*$_{(F2)}$/VEH and *Gif-/-*$_{(F2)}$/TAU mice (WT values set at 1 for each region). (E) Staining and quantification of alkaline phosphatase (ALP) activity in primary osteoblasts (Top panels) following 2 weeks treatment with vehicle or 20 mM taurine in osteogenic conditions (n=3) or staining and quantification of alizarin red (AR) in osteoblasts (Bottom panels) following 4 weeks treatment with vehicle or 20 mM taurine in osteogenic conditions (n=3). (F) Gene expression analysis of bone marker genes in WT, *Gif-/-*$_{(F2)}$/VEH and *Gif-/-*$_{(F2)}$/TAU mice. (G) Serum Ocn levels in WT, *Gif-/-*$_{(F2)}$/VEH and *Gif-/-*$_{(F2)}$/TAU mice. (H-I) Changes in IGF1R and ERK phosphorylation (H) and *Ccnd1* expression (I) in long bone collected from 8 weeks-old WT mice treated for 4 weeks with vehicle, Taurine (500mg/kg/day) or Taurine (500mg/kg/day) +OSI906 (50mg/kg/day). Lanes shown in Western blots of panel H were run contiguously, and blots were stripped and reprobed with IGFR or ERK. Relative quantification of pIGFR normalized to IGFR and pERK normalized to ERK is shown below each lane. A representative gel from 2 independent experiments is shown. (J) Growth plate thickness analysis in WT, *Gif-/-*$_{(F2)}$/VEH, *Gif-/-*$_{(F2)}$/B_{12} and *Gif-/-*$_{(F2)}$/TAU mice (n=5, each). All panels * $P < 0.05$; ♯ $P < 0.01$. U.D., undetectable. Error bars: SEM.

Figure S7

A

B_{12} deficiency in children due to maternal B_{12} deficiency

Control Group		S1	S2	S3	S4	S5	S6	S7	Mean±sem
Offspring		S1O	S2O	S3O	S4O	S5O	S6O	S7O	
	Age(months)	8	3	11	14	10	9	10.5	
	B_{12}(pmol/L)	394	171	280	346	394	163	264	287.8 ±36.5
	Taurine (μmol/L)	320	246	200	301	330	298	309	286.3 ±46.5
	Ocn (ng/ml)	107	82	140	100	110	99	103	105.9 ±17.5
	Anemia	-	-	-	-	-	-	-	
Mother		S1M	S2M	S3M	S4M	S5M	S6M	S7M	
	B_{12}(pmol/L)	ND	ND	182	ND	152	191	ND	175.3±9.47
	Anemia	-	-	-	-	-	-	-	

B_{12} deficient		S8	S9	S10	S11	S12	Mean±sem
Offspring		S8O	S9O	S10O	S11O	S12O	
	Age(months)	2	12	8	19	9	
	B_{12}(pmol/L)	117	37	44	61	37	59.3±15.2*
	Taurine (μmol/L)	196	120	111	148	109	136.8±36.6*
	Ocn (ng/ml)	21	40	37	49	36	36.7±10.2*
	Anemia	+	+	+	+	+	
Mother		S8M	S9M	S10M	S11M	S12M	
	B_{12}(pmol/L)	ND	78	128	105	113	106.4±9.1*
	Anemia	+	+	+	+	+	

C

B_{12} deficiency in aged population

	Healthy subjects	B_{12} deficient
n	10	8
Age	55.78 ± 3.58	55.17 ± 2.09
B_{12} (pmol/L)	448.5 ± 38.1	100.3 ± 12.6*
Taurine (μmol/L)	43.3 ± 3.3	30.3 ± 2.3*
Ocn (ng/ml)	7.2 ± 0.60	3.8 ± 0.40*
% Smokers	66.67	25.00
BMI (kg/m2)	25.35 ± 2.42*	29.27 ± 3.08
Calcium (mmol/L)	1.19 ± 0.06	1.21 ± 0.05
CRP (mg/L)	1.39 ± 0.85	2.07 ± 1.74
alcohol intake (g/wk)	64.00 ± 106.47	101.76 ± 152.35
Dyastolic pressure	92 ± 11.24	91.29 ± 13.58
Systolic pressure	142 ± 19	135 ± 13
Albumin (g/l)	41 ± 3.52	44.13 ± 3.13
T-Cholesterol (nmol/L)	5.36 ± 0.57	5.82 ± 0.91
Testosterone (mmol/L)	23.01 ± 7.13	20.70 ± 4.61
Hb (g/L)	145 ± 6.74	151 ± 9.44
P-Sodium(pg/mL)	141 ± 1.32	141.13 ± 2.16
P-Potasium(pg/mL)	4.0 ± 0.29	3.88 ± 0.28
CS-Uric acid (mmol/L)	0.01 ± 0.06	0.36 ± 0.03
S-Creatinine (umol/L)	91.5 ± 13.18	88.5 ± 8.82
DU-Creatinine (umol/L)	13.7 ± 3.3	14.7 ± 1.43
S-Ferritin (ug/L)	167.36 ± 101.80	194.75 ± 190.56

B

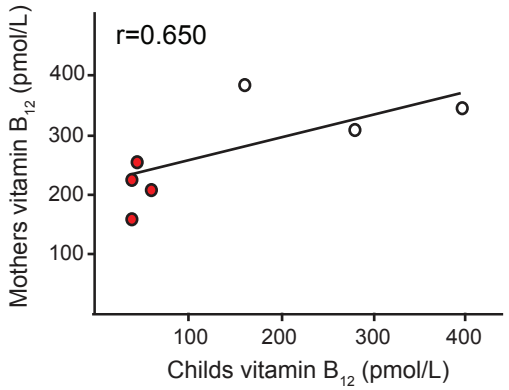

Supplementary figure 8. Vitamin B_{12} status correlates with taurine and the bone formation marker osteocalcin during early postnatal life and ageing in humans

(A) Clinical characteristics of controls and B_{12} deficient mothers and their children analyzed. Offspring (O) and corresponding mother (M) in control and B_{12} deficient groups are shown one above the other and have the same subject (S) number. Values are shown as average ±SEM. * $P < 0.01$. Healthy controls (n=7) and B_{12} deficient children (n=5). (B) Correlation analysis between mothers and childs vitamin B_{12} levels. Please note that these values are derived from panel A; some mother child correlations were not available as mothers did not provide blood samples. Pearson coefficient (r) values is shown. Red circles are values from children born from B_{12} deficient mothers and white circles are from healthy mothers. + indicates present, - indicates not present and ND indicates not determined.

(C) Clinical characteristics of aged controls and patients analyzed. BMI, body mass index. Values are shown as mean ±SEM. * $P < 0.01$.

Figure S8

METHODS

Micro-computed tomography (µCT) analysis

Trabecular bone and cortical architecture of the proximal tibia (secondary spongiosa) was assessed using a µCT system (Skyscan 1172). Tibia bone specimen was stabilized with gauze in a 2 ml centrifuge tube filled with 70% ethanol and fastened in the specimen holder of the µCT scanner. One hundred µCT slices, corresponding to a 1.05 mm region distal from the growth plate, were acquired at an isotropic spatial resolution of 10.5 µm. A global thresholding technique was applied to binarize gray-scale µCT images where the minimum between the bone and bone marrow peaks in the voxel gray value histogram was chosen as the threshold value. The trabecular bone compartment was segmented by a semi-automatic contouring method and subjected to a model-independent morphological analysis (Hildebrand et al., 1999) by the standard software provided by the manufacturer of the µCT scanner. 3D morphological parameters, including model independent measures by distance transformation (DT) of bone volume fraction (BV/TV), Tb.Th* (trabecular thickness), Tb.N* (trabecular number), Tb.Sp* (trabecular separation) and connectivity density (Conn.D) were evaluated. The Conn.D is a quantitative description of the trabecular connection (Feldkamp et al., 1989; Gundersen et al., 1993)

Cell cultures

Primary osteoblasts were cultured as previously described (Yadav et al., 2008). All the drug treatments were performed in serum free and B_{12} deficient medium unless stated otherwise. Cell proliferation was quantified by BrdU; differentiation by alkaline phosphatase activity assays; and mineralization by Alizarin red staining. Bromodeoxy Uridine (BrdU) cell proliferation assay: MC3T3 or primary osteoblast cells obtained from calvaria following standard protocol (Divieti et

al., 1998) were trypsinized, and 5000 cells/well were seeded in 96-well plate in B_{12}-deficient α-MEM. 24 hours cells after serum withdrawal cells were treated with B_{12} (1-10,000 nM) or vehicle and cells were left for another 24 hours in B_{12}-deficient α-MEM (0% FBS). For the last 4 hours of the 24-hour stimulation period, the cells were pulsed with BrdU. BrdU incorporation was measured using ELISA kit (Roche, IN, USA). Alkaline phosphatase (ALP) activity assay: MC3T3 or primary cells were trypsinized, 5000 cells/well were seeded onto 96-well plates, and treated with CN-B_{12} (1, 10 and 100 nM) for 48 hours in osteoblast differentiation medium containing B_{12}-deficient α-MEM, 10mM β-glycerophosphate, 50 mg/mL of ascorbic acid, and 1% penicillin/streptomycin. At the end of incubation period, total ALP activity was measured using p-nitrophenylphosphate (PNPP) as substrate, and absorbance was read at 405 nm.

RNA isolation and quantitative PCR analysis.

Total RNA was isolated using Trizol reagent (Sigma), DNase I treated and reverse transcribed with random primers using the Superscript III first-strand cDNA synthesis kit (Invitrogen, Carlsbad, CA). The cDNA samples were then used as templates for qPCR analysis, which was performed on an ABI real-time PCR machine instrument (ABI) using primers from SABiosciences (Frederick, MD) and the Taq SYBR Green supermix with ROX (Biorad, Hercules, CA). All primer sequences are available upon request. Expression levels of the studied gene were normalized using the GAPDH expression levels as internal control for each sample.

Genotyping of *Gif* mice

Genotyping was done on ear DNA samples using the primers: WT PCR (Forward Primer: TCTTCTCGGGGATCAAGAGC; Reverse Primer: GTCACCTTGGTCTTCCCAGC) and knock

out PCR (Forward Primer: ATCACGACGCGCTGTATC; Reverse Primer: ACATCGGGCAAATAATATCG) using standard PCR conditions.

Metabolomics analysis

Chemicals and reagents

All the metabolite standards, ammonium formate, ammonium acetate and ammonium hydroxide were obtained from Sigma-Aldrich (Helsinki, Finland). Formic acid (FA), 2-proponol, acetonitrile (ACN), and methanol (all HiPerSolv CHROMANORM, HPLC grade, BDH prolabo,) were purchased from VWR International (Helsinki, Finland). Isotopically labeled internal standards were obtained from Cambridge Isotope Laboratory. Inc., USA (Ordered from Euroiso-Top, France). Deionized Milliq water up to a resistivity of 18 MΩ was purified with a purification system (Barnstead EASYpure RoDi ultrapure water purification system, Thermo scientific, Ohio, USA).

Metabolite extraction protocol

The working calibration solutions were prepared in 96-well plate by serial dilution of the stock calibration mix using Hamilton's MICROLAB® STAR line (Hamilton, Bonaduz AG, Switzerland) liquid handling robot system. Starting from a stock solution mix, 10 additional lower working solutions were prepared using water as the diluent to build the calibration curves.

Liver:

Frozen liver samples were weighed (20 – 40 mg) and transferred to precellys homogenization tubes (Precellys 24 lysing kit, precellys) containing 1.4 mm ceramic (Zirconium oxide) beads by adding 10 uL of labeled internal standard mix and incubated on ice for 10 min. After incubation, 20 parts

of extraction solvent was added to the sample (1:20, sample:extraction solvent). In order to gain maximum recovery of small molecules, the homogenizations were performed with a Precellys 24 homogenizer (Precellys, Finland) in a two-step extraction process. In the first step, 10 parts of precooled 100% ACN + 1% FA was added to the sample and homogenized for 3 cycles of 20 sec each at 5,500 rpm with 30 sec pause between each homogenization interval. After homogenization, the sample tubes were centrifuged for 2 min at 5000 rpm at -2° C in an Eppendorf 5404R centrifuge and the supernatant was collected in a 1.5 ml eppendorf tube. In the second step, 10 parts of 80/20% ACN/H_2O + 1% FA was added to the remaining pellet and repeated the steps as above and finally pooled to the previous extract.

Cells:

Around two million cells per sample were taken for metabolomics analysis. Trypsinised cells were washed twice with PBS buffer and then with deionized water for few seconds. Subsequently cells were quickly quenched in liquid nitrogen and stored at -80°C until further analysis. Frozen cell samples were thawed step wise at -20°C and 4°C and then metabolites were extracted by adding 20 µL of labeled internal standard mix and 1 ml of cold extraction solvent (80/20 ACN/H2O + 1% FA). Cells were then sonicated for 30 sec, vortexed for 30 sec, and incubated on ice for 10 min. After the centrifugation supernatants were aspirated into eppendorf tubes.

Clinical serum samples:

Ten microliters of labeled internal standard mixture was added to 100 µL of serum sample. Taurine was extracted by adding 4 parts (1:4, sample:extraction solvent) of the 100% ACN + 1% FA solvent. The collected extracts were dispensed in OstroTM 96-well plate (Waters Corporation,

Milford, USA) and filtered by applying vacuum at a delta pressure of 300-400 mbar for 2.5 min on robot's vacuum station. This resulted a cleaner extract to the 96-well collection plate, which was placed under the OstroTM plate. The collection plate was sealed with the cap map and placed in auto-sampler of the LC system for the injection.

Instrumentation and analytical conditions

Sample analysis was performed on an ACQUITY UPLC-MS/MS system (Waters Corporation, Milford, MA, USA). The auto-sampler was set at 5°C, and the column, 2.1 × 100 mm Acquity 1.7um BEH amide HILIC column (Waters Corporation, Milford, MA, USA), temperature was maintained at 45°C. The total run time is 14.5 min including 2.5 min of equilibration step at a flow rate of 600 µL/min. Initially the gradient started with a 2.5 min isocratic step at 100% mobile phase B (ACN/ H_2O, 90/10 (v/v), 20 mM ammonium formate, pH at 3), and then rising to 100% mobile phase A (ACN/H_2O, 50/50 (v/v), ammonium formate, pH at 3) over the next 10 min and maintained for 2min at 100% A and finally equilibrated to the initial conditions for 2.5 min. An injection volume of 5 µL of sample extract was used and two cycles of 300 µL of strong wash (methanol/isopropanol/ACN/H_2O, 25/25/25/25, 0.5% FA) and 900 µL of weak wash (methanol/isopropanol/ACN/H_2O, 25/25/25/25, 0.5% ammonium hydroxide) and in addition 2 min of seal wash (90/10, methanol/H_2O) were carried out. The auto-sampler was used to perform partial loop with needle overfill injections for the samples and standards.

The detection system, a Xevo® TQ-S tandem triple quadrupole mass spectrometer (Waters, Milford, MA, USA), was operated in both positive and negative polarities with a polarity switching time of 20 msec. Electro spray ionization (ESI) was chosen as the ionization mode with a capillary

voltage at 0.6 KV in both polarities. The source temperature and desolvation temperature of 120°C and 650°C, respectively, were maintained constantly throughout the experiment. Declustering potential (DP) and collision energy (CE) were optimized for each compound. High pure nitrogen and argon gas were used as desolvation gas (1000 L/hr) and collision gas (0.15 ml/min), respectively. Multiple Reaction Monitoring (MRM) acquisition mode was selected for quantification of metabolites with individual span time of 0.1 sec given in their individual MRM channels. The dwell time was calculated automatically by the software based on the region of the retention time window, number of MRM functions and also depending on the number of data points required to form the peak. MassLynx 4.1 software was used for data acquisition, data handling and instrument control. Data processing was done using TargetLynx software and metabolites were quantified by using labeled internal standards and external calibration curves.

Metabolomics data analysis

Metabolomics data analysis was carried out using a web-based comprehensive metabolomics data processing tool, MetaboAnalyst 2.0 (http://www.metaboanalyst.ca) (Xia et al., 2009 and 2012). Briefly, in order to identify biologically meaningful patterns based on the metabolomics data, quantitative enrichment analysis (QEA) was carried out. Data was mapped according to human metabolome database and "metabolic pathway associated metabolite sets" library with 88 metabolite sets based on normal metabolic pathways was chosen for QEA. Next, in order to identify which metabolic pathways are significant with "hub" nodes, metabolic pathway topological analysis was carried out. For this pathway enrichment analysis (PEA), quantitative data was mapped and mouse metabolite pathway library with 82 entries was selected. The other parameters chosen were, global test and betweenness centrality node measurement. The PEA results were

displayed as metabolome view graph. In order to identify the clustering patterns among the metabolites and samples, 2-way hierarchical cluster analysis was done. For this purpose, quantitative data was autoscaled i.e., mean-centered and divided by the standard deviation of each variable. Dendrogram was plotted on normalized data using Ward's linkage clustering algorithm and Pearson's correlation similarity measure. Dendrogram was visualized as heatmap, where each coloured cell on the map corresponds to a concentration value. In order to analyze differences among groups, univariate analysis one-way analysis of variance (ANOVA) was performed on autoscaled data. In order to explain the maximum separation among groups, supervised multivariate regression technique, partial least squares discriminant analysis (PLS-DA) was performed. Non-transformed data was mean-centered and divided by standard deviation of each variable (autoscaled). The number of latent variables (LVs) to be used to build a PLS-DA model depend on the sum of squares captured by the model (R^2) and cross-validated R^2 (Q^2). Five components were used in all the PLS-DA models. Leave one out cross-validations (LOOCV) were used to validate the models. Variable importance in projection (VIP) is one of the important measures of PLS-DA, where it is a weighted sum of squares of the PLS loadings taking into account the amount of explained class variation in each dimension. Metabolites were ranked according to their VIP scores and usually metabolites with VIP scores greater than one are considered as the most significant contributors. Unsupervised multivariate analysis, Principle component analysis (PCA), and Spearman correlations between metabolites were done using MetaDAR package (http://code.google.com/p/metadar).

REFERENCES:

Divieti, P., Lanske, B., Kronenberg, H.M., and Bringhurst, F.R. (1998). Conditionally immortalized murine osteoblasts lacking the type 1 PTH/PTHrP receptor. Journal of bone

and mineral research : the official journal of the American Society for Bone and Mineral Research *13*, 1835-1845.
Feldkamp, L.A., Goldstein, S.A., Parfitt, A.M., Jesion, G., and Kleerekoper, M. (1989). The direct examination of three-dimensional bone architecture in vitro by computed tomography. J Bone Miner Res *4*, 3-11.
Gundersen, H.J., Boyce, R.W., Nyengaard, J.R., and Odgaard, A. (1993). The Conneulor: unbiased estimation of connectivity using physical disectors under projection. Bone *14*, 217-222.
Hildebrand, T., Laib, A., Muller, R., Dequeker, J., and Ruegsegger, P. (1999). Direct three-dimensional morphometric analysis of human cancellous bone: microstructural data from spine, femur, iliac crest, and calcaneus. J Bone Miner Res *14*, 1167-1174.
Yadav, V.K., Ryu, J.H., Suda, N., Tanaka, K.F., Gingrich, J.A., Schutz, G., Glorieux, F.H., Chiang, C.Y., Zajac, J.D., Insogna, K.L.*, et al.* (2008). Lrp5 controls bone formation by inhibiting serotonin synthesis in the duodenum. Cell *135*, 825-837.